CAVITY SHIFTS OF MEASURED ELECTRON MAGNETIC MOMENTS

Gerald Gabrielse* and Joseph Tan*
Department of Physics
Harvard University
Cambridge, MA 02138

Lowell S. Brown**
Department of Physics
University of Washington
Seattle, WA 98195

Contents

1. Introduction and history 2
2. One-electron cyclotron oscillator 3
3. Simple model 6
4. Cylindrical, spherical cavities and hyperbolic cavities 11
   a. Cylindrical cavity 12
   b. Spherical cavity 15
   c. Hyperbolic cavity 15
5. Implications for present experiments 16
6. Renormalized calculation of cavity shifts 18
   a. Renormalization 18
   b. Spherical cavity 21
   c. Cylindrical cavity 22
7. Summary and future prospects 24
8. References and footnotes 26
9. Appendix: tabulated cavity properties 28

To appear in **Quantum Electrodynamics**, edited by T. Kinoshita, (World Scientific, Singapore, 1990)

* Supported by the U.S. National Science Foundation.
** Supported by the U.S. Department of Energy.

1. Introduction and History

The measured magnetic moment of the electron provides the most accurate test of quantum electrodynamics.[1,2] Until a few years ago, the measurements were conceptually simple, with no large systematic corrections required. However, the accuracy of the experiments has improved to the extent that this is no longer true. Presently, the measurements utilize line splitting based upon an intricate theory of the observed line shape[3] . The experimental accuracy is limited by a lack of control over the interaction of a single electron oscillator with the electromagnetic modes of a surrounding microwave cavity. (The unavoidable cavity in experiments so far is formed by the metal electrodes of the Penning trap used to confine the electron.) Efforts are underway to remove the reliance upon the theory of the observed resonance line. One possibility is to switch on and off the inhomogeneous magnetic field which both makes possible and limits the current experiments.[2] Another possibility is to utilize relativistic couplings which have been observed[4] to avoid the noise broadened lineshape which is an unpleasant consequences of the magnetic field inhomogeneity. Whatever approach succeeds, possible cavity shifts of the measured magnetic moment (the subject of this chapter) must be controlled or eliminated if further experimental progress is to be made.

The possibility of cavity shifts of the measured cyclotron frequency used to determine an electron's magnetic moment was first demonstrated when the coupling of the electron oscillator and a trap cavity was directly observed by Gabrielse and Dehmelt.[5] The first of the reported observations was made almost a year and one half before they were published. The reason for the delay illustrates a difficulty in performing these measurements. A proper study required shifting the electron cyclotron frequency by changing the current in a superconducting solenoid and this was delayed to avoid the long time (up to a month) required for the field to restabilize sufficiently to allow more measurements. During this year and a half, estimates with electrical analogs[6] and an explicit model calculation[7] were undertaken to estimate the size of possible cavity shifts. Eventually, the observation of a coupling between an electron and a trap cavity was repeated at one electron frequency in another trap.[2] In hindsight, it is now clear that the cavity coupling is responsible for a slower than expected decay of the electron's cyclotron motion which had earlier been attributed to electronic causes.

Although the importance of cavity shifts for measurements of the electron magnetic moment was realized only recently, the basic notion that the couplings of two oscillators can shift both the damping rate and oscillation frequency of the oscillations is certainly very familiar. (The electron in its cyclotron motion and the electromagnetic cavity modes are the coupled oscillators here.) Long ago, for example, it was mentioned that the spontaneous emission of an atom placed in a cavity could be inhibited.[8] Further discussions of cavity-induced modifications to atom damping rates came later,[9] with clear realization of the problems that the frequency shifts would present for precise measurements of resonance frequencies.[10] In fact, the observation of inhibited spontaneous emission in a trap was the first observation of inhibited spontaneous emission in a cavity. Soon after, similar effects were observed with Rydberg atoms and now a variety of such studies have been carried out.[11]

The electron cyclotron oscillator and the observed coupling to a trap cavity are introduced in Sec. 2. Only a pure cyclotron motion is considered because other aspects of the motion of a single particle in a Penning trap are well understood[12] and do not complicate our examination of damping and frequency shifts. A simple model, wherein an electron oscillator is coupled to an LCR circuit which represents a single cavity mode, is developed in Secs. 3 and 4. The simple model is useful for understanding and for estimating changes in the damping rate and the resonance frequency of the electron oscillator. It is qualitatively useful as well, when the cyclotron oscillator is near to resonance with a cavity mode. In Sec. 4, eigenmodes of cylindrical, hyperbolic and spherical cavities are examined. Calculated coupling coefficients are presented which indicate how well each mode couples to an electron cyclotron motion around the symmetry axis of the cavity at its center. Sufficient information is provided so that the coupling of any of the cavity modes to the electron oscillator can be treated using the simple model. The way that cavity shifts limit the current measurements of the electron magnetic moment is discussed in Sec. 5. Only the simple model is used, given the limited experimental information which makes a more detailed theoretical analysis to be unwarranted.

Unfortunately, the simple model is not a complete description, especially when the electron cyclotron oscillator is not near to resonance with a high Q cavity mode. In fact, the sum of frequency shifts computed with the simple model diverges if contributions from too many cavity modes are included. Rigorous calculations are thus required to establish the validity and limitations of the simple model.[13] Detailed, renormalized calculations for a cylindrical cavity[14] and a spherical cavity[15] are reviewed in Sec. 6. These calculations are classical since it has been shown that within a high level of accuracy, the exact apparatus of quantum electrodynamics yields the classical results.[16] A comparison of the exact cylindrical calculation with the simple model has been used to justify an approximate treatment of the hyperbolic cavity, for which a more exact calculation cannot be done.[13] Finally, future possibilities for dealing with cavity shifts are discussed in Sec. 7. Particular attention is paid to a cylindrical microwave cavity[17] since it has recently been demonstrated that a single electron can be accurately studied with trap electrodes which approximate this configuration,[18] just as well as within the customary hyperbolic electrodes.

The present state of experimental information about the cavity modes and how much they affect the measurements of the electron magnetic moment is far from satisfactory. Ideally, the magnetic moment would be measured over a wide range of electron cyclotron frequencies, a range over which the location, Q and symmetry of cavity modes is well known (instead of at only a single frequency). Although there is now some experimental indication of the location and Q of cavity modes,[2,19] the estimates in this article are badly in need of more experimental information. Hopefully, the estimates will be replaced by measurements.

2. One-electron Cyclotron Oscillator

For our purposes it suffices to deal with a cyclotron motion of an electron (of charge e and mass m) in a uniform magnetic field B. In free space, the electron orbits a magnetic field line at angular frequency (CGS units)

$$\omega_c = \frac{eB}{mc} \tag{1}$$

This cyclotron motion is damped via synchrotron radiation with a damping width

$$\gamma_c = \frac{4e^2\omega_c^2}{3mc^2} \tag{2}$$

which is just the ratio of the power radiated from the circular motion (given by the familiar Larmor formula) divided by the instantaneous energy stored in this motion. Typically, the cyclotron motion is damped only very weakly so that the radiation width is very much smaller than the cyclotron frequency. For $B = 5.9$ Tesla, for example, $\omega_c/2\pi = 164$ GHz and $\gamma_c/2\pi = 1.3$ Hz so that

$$\frac{\gamma_c}{\omega_c} = 8 \times 10^{-12}. \tag{3}$$

Without line splitting, therefore, the cyclotron frequency could (in principle) be measured to 8×10^{-12}. The corresponding decay time is $\tau_c = \gamma_c^{-1} = 100$ ms.

To relate the uncertainty $\Delta\omega_c$ in measuring the cyclotron frequency to the resulting uncertainty Δa in the measured anomalous magnetic moment a which is so important for tests of quantum electrodynamics, we note that

$$a = \frac{\omega_s - \omega_c}{\omega_c} \tag{4}$$

can be regarded as a definition of a, where ω_s is the electron's spin precession frequency. Since $a \approx 10^{-3}$ is small,

$$\frac{\Delta a}{a} \approx \frac{1}{a}\frac{\Delta\omega_c}{\omega_c}. \tag{5}$$

Setting $\Delta\omega_c$ equal to the free space line width yields $\Delta a/a \approx 8 \times 10^{-9}$. The experimental error currently quoted[2] is half this amount.

Both the cyclotron frequency and the damping rate can be shifted when the one electron cyclotron oscillator is located within a microwave cavity rather than in free space. Fig. 1 shows the cavity within which the the inhibition of spontaneous emission was first observed. Fig. 2 shows measured cyclotron damping times[5] of 86 ± 2 and 347 ± 64 ms for cyclotron frequencies which differ by only 0.5%. These are the first observations of damping times which differ from the $\tau_c = 100$ ms expected for radiation into free space from Eq. (2). The damping clearly varies as the electron cyclotron frequency (and hence the detuning from the nearest eigenmode of the trap cavity) is changed. The longest damping time observed in this particular trap was about three times longer than the damping time for free space. This first observation was subsequently repeated in another trap[2], but with a damping time $\tau = \gamma^{-1} = 1.0 \pm 0.1s$, about 10 times larger than in free space.

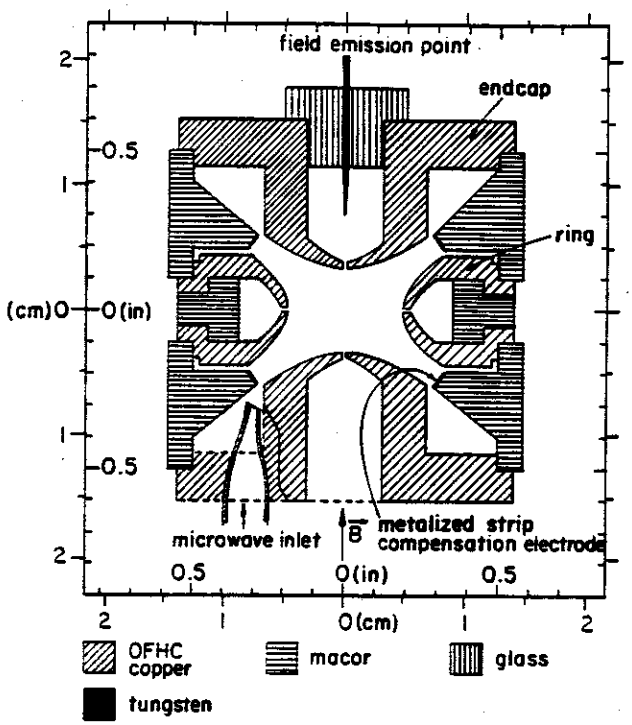

Fig. 1. Hyperbolic Penning Trap in which the inhibited spontaneous emission of a one-electron cyclotron oscillator was first observed. (From Ref. 5.)

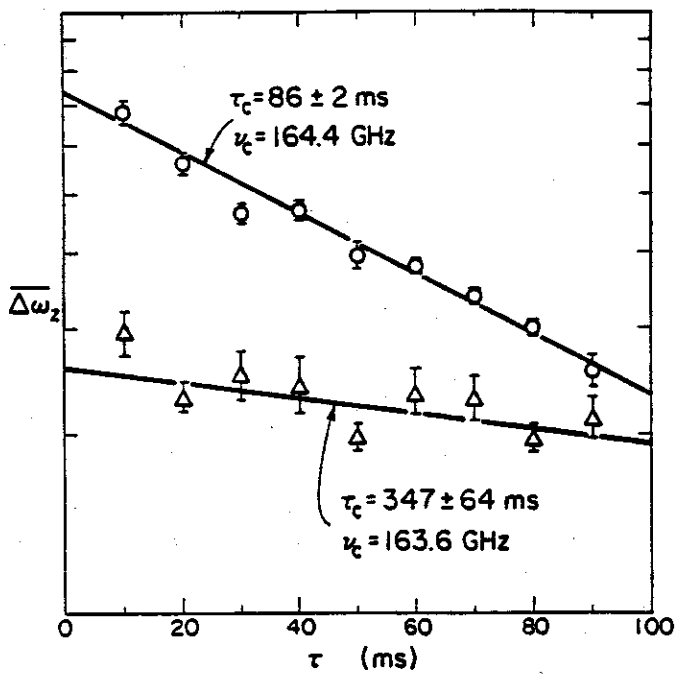

Fig. 2. Measured decay of the energy of a one-electron cyclotron oscillator in the trap of Fig. 1 as a function of time for two electron cyclotron frequencies which differ by only 0.5 %. Both damping times differ from the free space value $(\gamma_c)^{-1} = 0.1$ s because of the microwave cavity formed by the trap electrodes. (From Ref. 5.)

3. Simple Model

To illustrate the characteristic way that the damping rate and resonant frequency of an electron cyclotron oscillator is modified by its interaction with a microwave cavity, we use the simple model in Fig. 3a. In this model, the N^{th} cavity mode is represented to the right by an LCR tuned circuit.[20] Such a circuit is resonant at angular frequency $\omega_N = (LC)^{-1/2}$ with damping width $\Gamma_N = (RC)^{-1}$. The electron oscillator is represented as a charge e and mass m on a spring with spring constant $m\omega_c^2$. The interaction between the LCR and the electron is via the force $-eV/d$ on the charge which occurs when a potential V is present across two extended plates (separated by an effective distance d) between which the particle is located. (The effective capacitance of the two plates is included in C.) The unperturbed resonance frequency of the two oscillators are related by a detuning δ defined by

$$\omega_c = \omega_N + \frac{1}{2}\Gamma_N\delta. \tag{6}$$

Presently we shall provide explicit expressions for the combination of the parameters L,C,R and d which will make the simple model quantitatively useful as well.

To emphasize that the cavity mode is in fact an oscillator, at any given frequency we can substitute an equivalent series $L_sC_sR_s$ circuit for the parallel LCR circuit as shown in Fig. 3b. We choose the same resonant frequency $\omega_N = (L_sC_s)^{-1/2}$, and the parallel and series circuits are indistinguishable at any given frequency provided that

$$L_s = -\frac{R_s}{\Gamma_N} \tag{7}$$

and

$$R_s = \frac{R}{1+\delta^2}. \tag{8}$$

The negative series inductance (and capacitance) signify an effective phase change and to simplify the latter expression we have assumed that $\delta << (2\omega_N/\Gamma_N)$. Both oscillators now explicitly satisfy harmonic oscillator equations

$$\ddot{z} + \omega_c^2 z = -\frac{eV}{md} \tag{9}$$

$$\ddot{q} + \frac{R_s}{L_s}\dot{q} + \frac{1}{L_sC_s}q = \frac{V}{L_s}, \tag{10}$$

where q is the charge stored in the capacitor and $\dot{q}$ denotes that q is differentiated with respect to time. The two equations are easily combined to eliminate V which couples them.

The remaining equation can be solved by inspection if the instantaneous power transfered from circuit to electron $-\dot{q}V$ is equated to the power dissipated by the electron $-eV\dot{z}/d$, yielding the Schotky formula

$$\dot{q} = \left(\frac{e}{d}\right)\dot{z}. \tag{11}$$

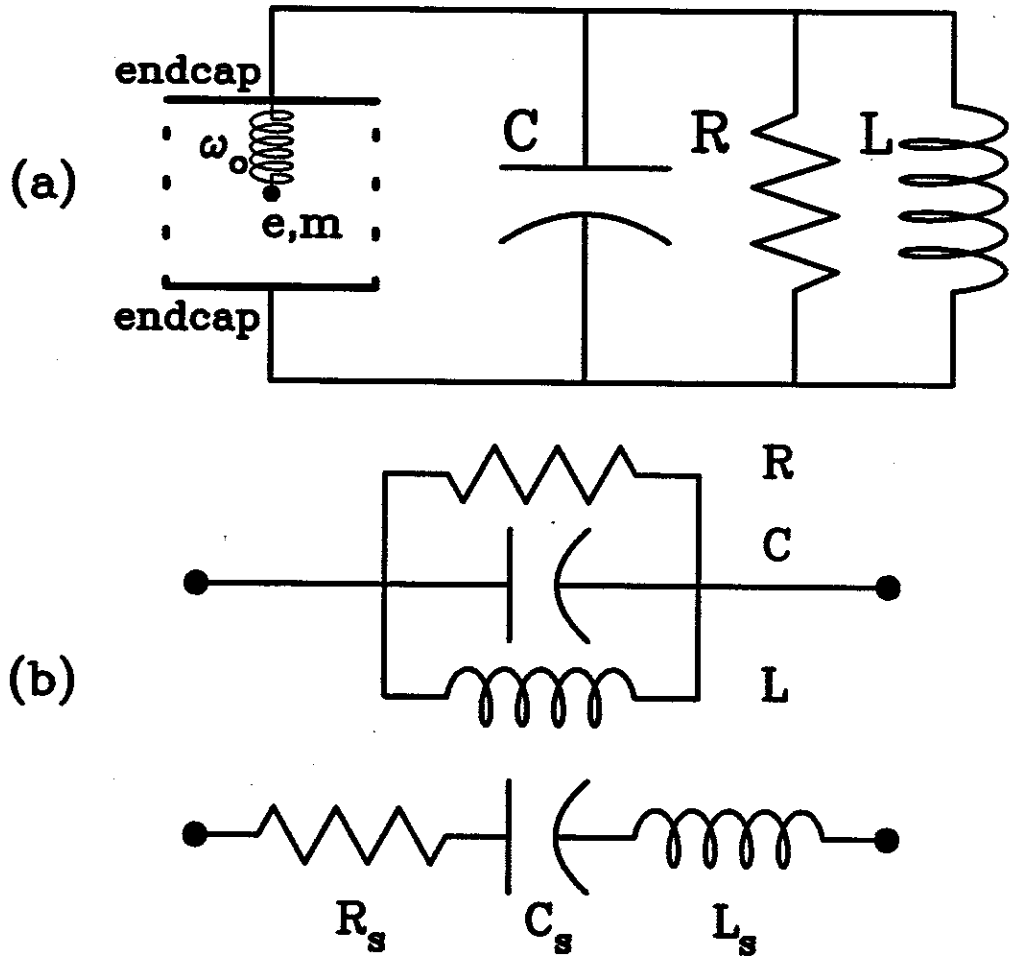

Fig. 3. (a) Simple model of the interaction of a one-electron cyclotron oscillator (represented as a charge e and mass m on a spring with spring constant $m\omega_c^2$) and a electromagnetic mode of a microwave cavity (represented as a parallel LCR circuit). (b) At any one frequency, the parallel LCR circuit may be represented as a series $L_sC_sR_s$ circuit.

We choose the origin of the coordinate system to coincide with the center of the trap so that $q = (e/d)z$ as well. The q dependence can then be eliminated to obtain a single damped harmonic oscillator equation

$$\ddot{z} + \gamma\dot{z} + (\omega_c + \Delta\omega)^2 z = 0 \tag{12}$$

which describes the motion of the coupled electron. The electron is damped via its coupling to the cavity mode at a rate

$$\gamma = \frac{\gamma_N}{1+\delta^2}. \tag{13}$$

The maximum damping rate γ_N (discussed in the next paragraph) pertains on resonance when ω_c and ω_N coincide (i.e. $\delta = 0$). The electron frequency is shifted from ω_c to $\omega_c + \Delta\omega$

with

$$\Delta\omega = \frac{\gamma_N}{2}\frac{\delta}{1+\delta^2} = \frac{1}{2}\gamma\delta. \tag{14}$$

If the electron oscillator and the LCR circuit are tuned to the same unperturbed resonance frequency (i.e. $\delta = 0$) there is no frequency shift. The maximum frequency shifts $\pm\gamma_N/4$ occur near resonance, at detunings $\delta = \pm 1$. The characteristic shapes for γ and $\Delta\omega$ are shown in Fig. 4 and these will be clearly evident in more detailed calculations which follow as well.

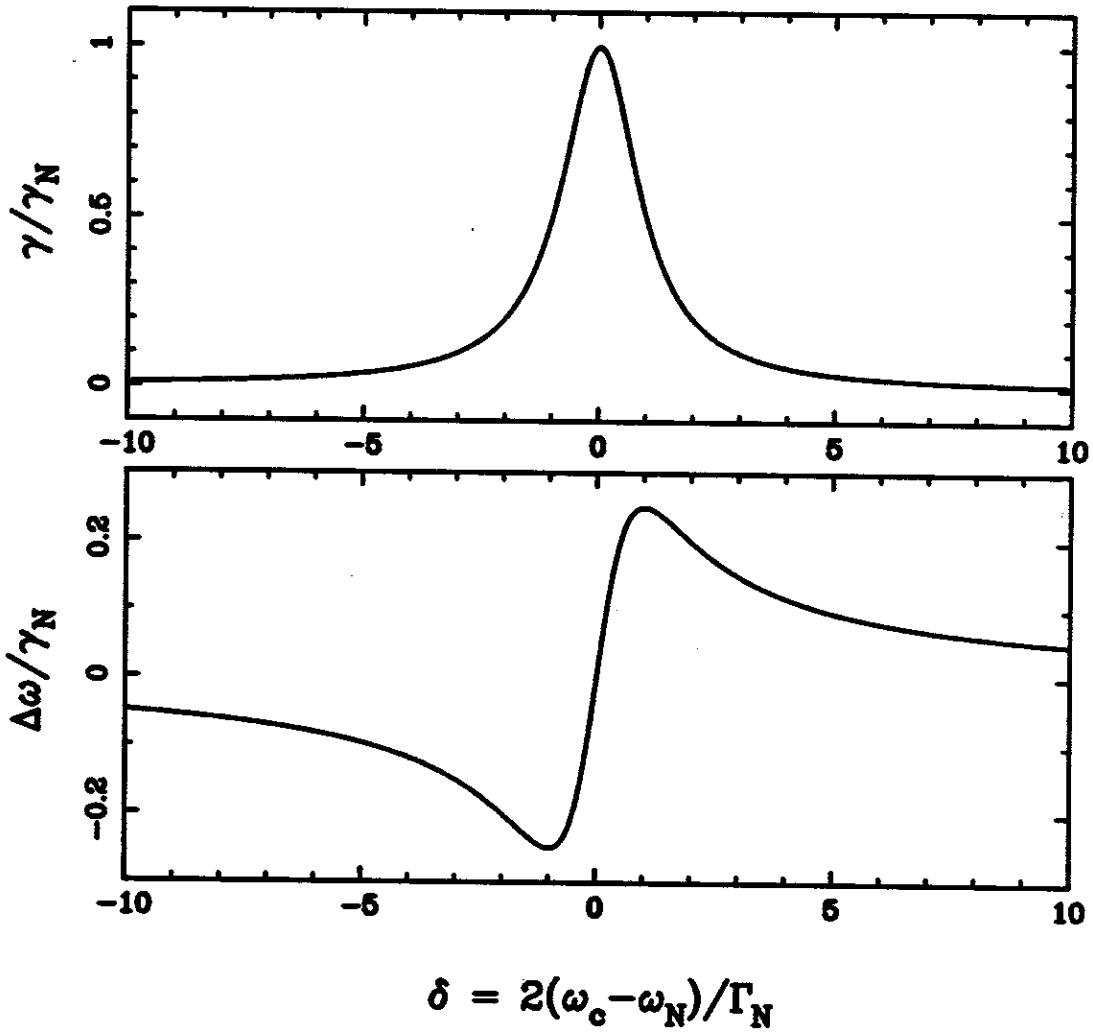

Fig. 4. Characteristic dependence of an oscillator's damping rate γ in (a) and frequency shift $\Delta\omega$ in (b) as a function of its detuning δ from the resonant frequency of an LCR circuit (or a cavity mode).

The maximum of the damping rate and the maximum of the frequency shift are both determined by

$$\gamma_N = \frac{e^2}{d^2}\frac{R}{m}. \tag{15}$$

Since $\gamma_N \sim R \sim Q_N$, the maximum damping and maximum frequency shift are larger when the quality factor $Q_N = \omega_N/\Gamma_N$ is larger. To display the Q dependence explicitly we write

$$\frac{\gamma_N}{\omega_N} = 2Q_N \left(\frac{\lambda_N}{\omega_N}\right)^2 \tag{16}$$

thereby defining the coupling strength[21] λ_N. This definition also allows the use of a simple form for the electron's frequency shift and damping rate

$$\Delta\omega - i\frac{\gamma}{2} = \frac{\omega(\lambda_N)^2}{\omega^2 + i\omega\Gamma_N - \omega_N^2}. \tag{17}$$

Using the parameters of the LCR model,

$$(\lambda_N)^2 = \frac{1}{2}\frac{r_e c^2}{Cd^2}, \tag{18}$$

where we have utilized the classical electron radius $r_e = e^2/mc^2$. Coupling strengths for cavities of interest will be specified in the next section.

To illustrate the results of the simple model, the solid lines in Fig. 5 represent the damping γ and frequency shift $\Delta\omega$ as a function of detuning δ (upper abcissa), for an electron cyclotron oscillator coupled to a mode of a cylindrical microwave cavity. (The mode eigenfrequency is within the frequency range where experiments are being done and the coupling strength used is described in the next section.) For comparison, the results of a more complete calculation (described in Sec. 6) are represented by the dotted line. For this relatively high Q value, $Q = 10^4$, the simple model describes both the damping and frequency shifts near the mode so well as to make the two curves almost indistinguishable.

Fig. 6 shows a similar comparison for a lower $Q = 1000$. Again the simple, one-mode model works very well near the mode. The larger frequency spread being viewed, however, reveals significant deviations between the one-mode model (solid lines) and the exact calculation (dotted lines). The major difficulty is the coupling of the electron to additional cavity modes which are nearby, as is illustrated at the left of the figure because of a nearby mode which is strongly coupled. These contributions can be largely accounted for by summing the contributions to γ and $\Delta\omega$ over additional, nearby modes. We thus replace Eq. (17) by the mode sum

$$\Delta\omega - i\frac{\gamma}{2} = \omega - \omega_c - i\frac{\gamma_c}{2} = \omega \sum_N \frac{\lambda_N^2}{\omega^2 + i\omega\Gamma_N - \omega_N^2}, \tag{19}$$

where the frequency of the cyclotron oscillator, ω, is now taken to be complex. The dashed line in Fig. 6 shows what happens when contributions are included from one additional cavity mode on either side. The agreement with exact values is much better, particularly at the left of the figure.

More than 3 modes are clearly required to describe the region between cavity modes with accuracy comparable to the experimental precision. The contributions to $\Delta\omega$ from off-resonant modes are clearly important, going as $\frac{1}{2}(\lambda_N)^2/(\omega_c - \omega_N)$, independent of Q_N.

Including the contribution of more modes to the mode sum does improve the agreement with the exact values. A careful study for $Q = 10^3$ shows that the agreement gets better as more modes are included up to approximately 7 modes to either side of the frequency being considered.[13] If more modes are included, however, the error in the frequency shift (i.e. in the real part of the mode sum) begins to increase. In fact, the frequency shift from the mode sum diverges if the mode sum includes all the cavity modes which couple to the electron cyclotron motion. This divergence, and how it can be correctly removed by renormalization in certain cases, is discussed in Sec. 6. A truncated mode sum was used to calculate the damping and frequency shifts of an electron cyclotron oscillator within a hyperbolic cavity,[13] since an exact calculation has not been feasible in this geometry.

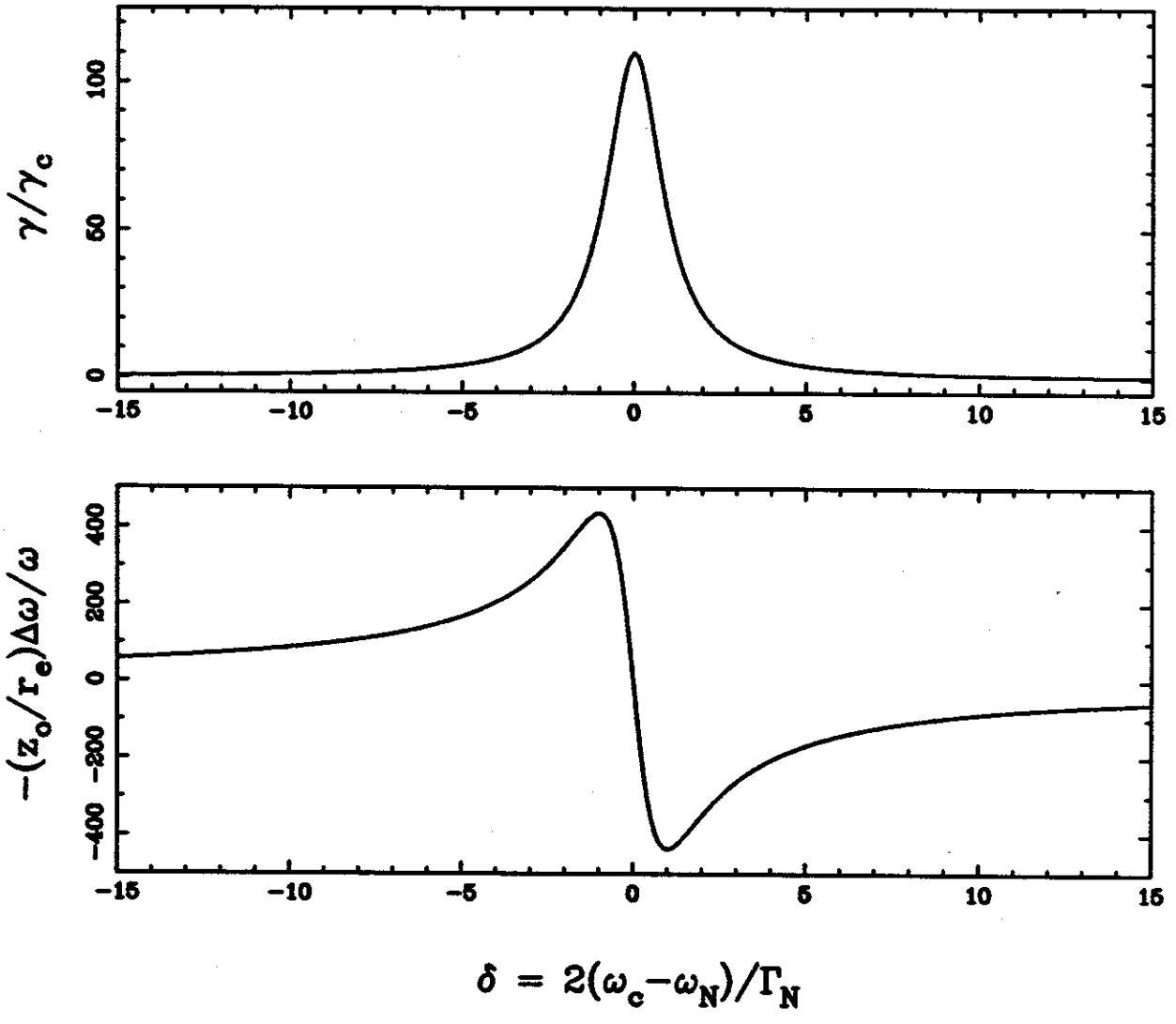

Fig. 5 The simple model and the exact calculation of Sec. 6 yield indistinguishable damping rate (above) and frequency shift (below) near a cylindrical cavity mode at $\xi_N \approx 3.781$ *with* $Q = 10^4$.

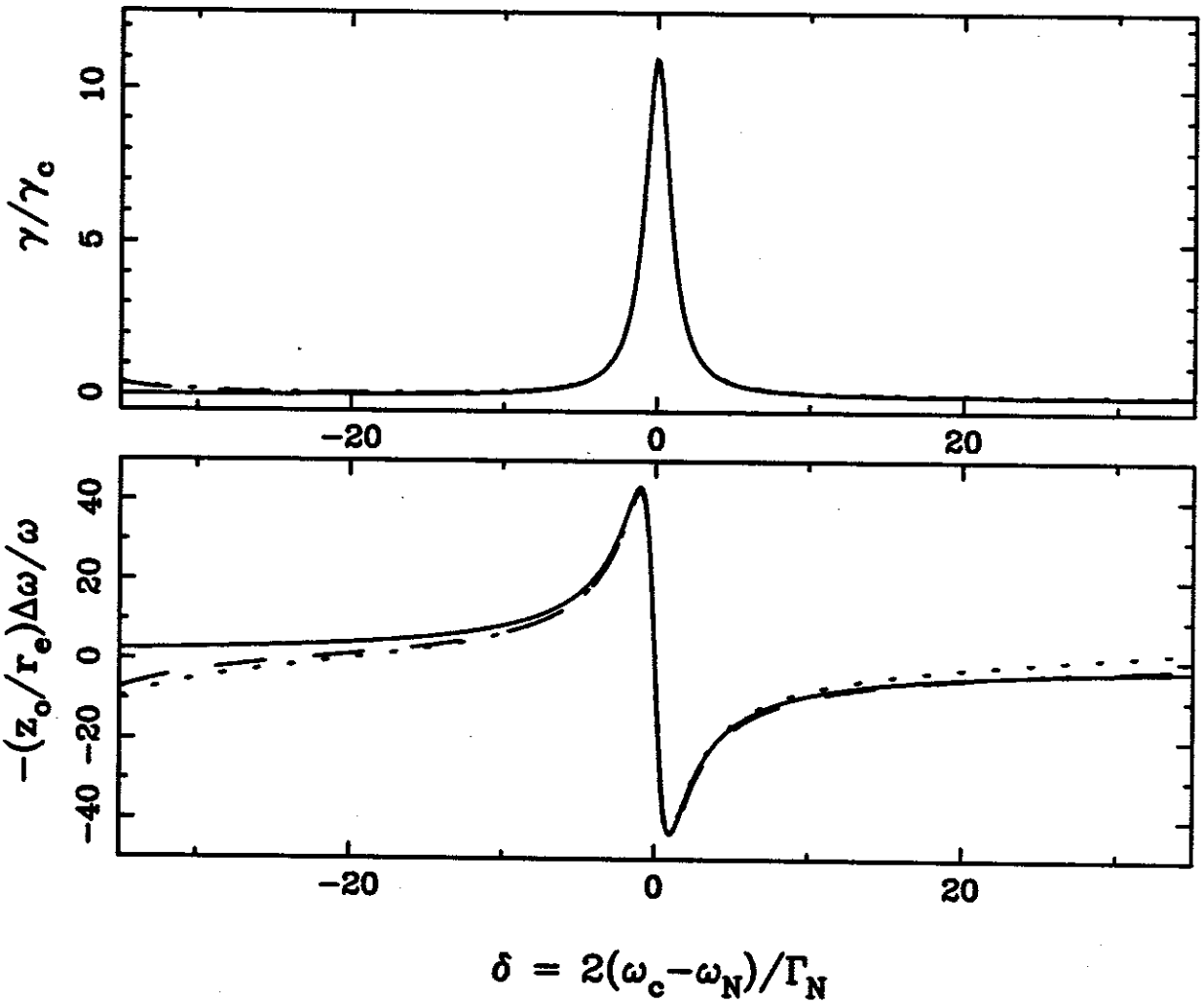

Fig. 6. Comparison of simple model (solid line) and the exact calculation of Sec. 6 (dotted line) for a cylindrical cavity mode at $\xi_N \approx 3.781$ with $Q = 10^3$. Adding the contributions of an additional cavity mode to either side (dashed line) improves the agreement.

4. Cylindrical, Hyperbolic and Spherical Cavities

To use the simple model to quantitatively describe the interaction of the electron cyclotron oscillator with a cavity mode, we must of course specify the resonant frequency ω_N and the quality factor $Q_N = \omega_N/\Gamma_N$ for the mode. Also, the coupling constant $(\lambda_N)^2$, which indicates the strength of the interaction between an electron and a cavity mode, must be specified. This is equivalent to specifying an effective value of Cd^2. We focus upon three cavity geometries of interest, considering only modes which couple to cyclotron motion about the symmetry axis of a single electron located at the center of the cavity. For each cavity geometry, the size of the cavity is indicated by an appropriately defined constant z_o. The use of a normalized frequency

$$\xi = \frac{2z_o}{\lambda} = \frac{z_o\omega}{\pi c} \tag{20}$$

which is independent of the overall size, makes it possible to separate out the dependence of the cavity properties on the cavity size.

The first cavity considered is a cylindrical cavity (Fig. 7) which is of particular interest because a one-electron cyclotron oscillator is being studied within a Penning trap whose electrodes approximate the idealized cavity shown in the figure. Also, a detailed calculation for this geometry (Sec. 6), makes it possible to establish the limitations of simple models. The second cavity discussed is a simple spherical cavity (Fig. 8). This cavity is included because its high degree of symmetry allows a particularly simple rigorous calculation of its effects upon a one-electron cyclotron oscillator located at its center. The third is a hyperbolic cavity (Fig. 9).. The traps used in the past to study one-electron cyclotron oscillators (including the trap used for the most precise electron magnetic moment measurement[2]) have electrodes which approximate equipotentials of an electric quadrupole potential which they are used to produce.

At the outset it is possible to estimate possible Q values. Up to a geometrical factor (which depends upon the specific field configuration of a particular cavity mode) the Q value is simply the ratio

$$Q \sim \frac{V}{A\delta_s} \sim \frac{z_0}{\delta_s}, \tag{21}$$

where V is the volume of the cavity and $A\delta_s$ is the penetration volume of the fields into the cavity walls. Here A is the interior surface area for the cavity and δ_s is the skin depth. The skin depth is related to the conductivity of the cavity walls and the angular frequency ω by

$$\delta_s = c/\sqrt{2\pi\omega\sigma}. \tag{22}$$

For a pure material like copper at low temperature ($T < 30\ K$), the electrical conductivity is very high ($\sigma > 10^{20}\ s^{-1}$) and the skin depth is very small ($\delta_s < 10^{-6}$ cm). This yields an estimate of $Q > 10^5$.

In practice, the Q values of the hyperbolic traps used so far seem to be lower. Holes and slits in the electrodes (to admit particles and to allow potentials to be applied to the trap electrodes) can allow radiation to leak out of the cavity, lowering the Q. In the only hyperbolic trap in which Q values were measured, Q values on the order of 1000 were indicated.[2] The Q value in the cylindrical trap now being used may well be higher, since choke flanges were incorporated to minimize the losses of radiation through the slits between electrodes. Unfortunately, the Q values are not yet well known and hence cannot be treated very accurately in any calculation.

a. Cylindrical Cavity

The cylindrical cavity represented in Fig. 7 is invariant under rotations about z-axis, with radial dimension ρ_o and axial dimension z_o. For numerical examples, we choose a relative geometry of $\rho_o/z_o = 1.186$ as indicated in Fig. 7, the choice which is used experimentally to provide optimum electrostatic properties for the Penning trap.[14] The well known mode eigenfrequencies are obtained by solving the boundary-value problem for perfectly conducting surfaces. To find the analytic expressions for C and d, however, we

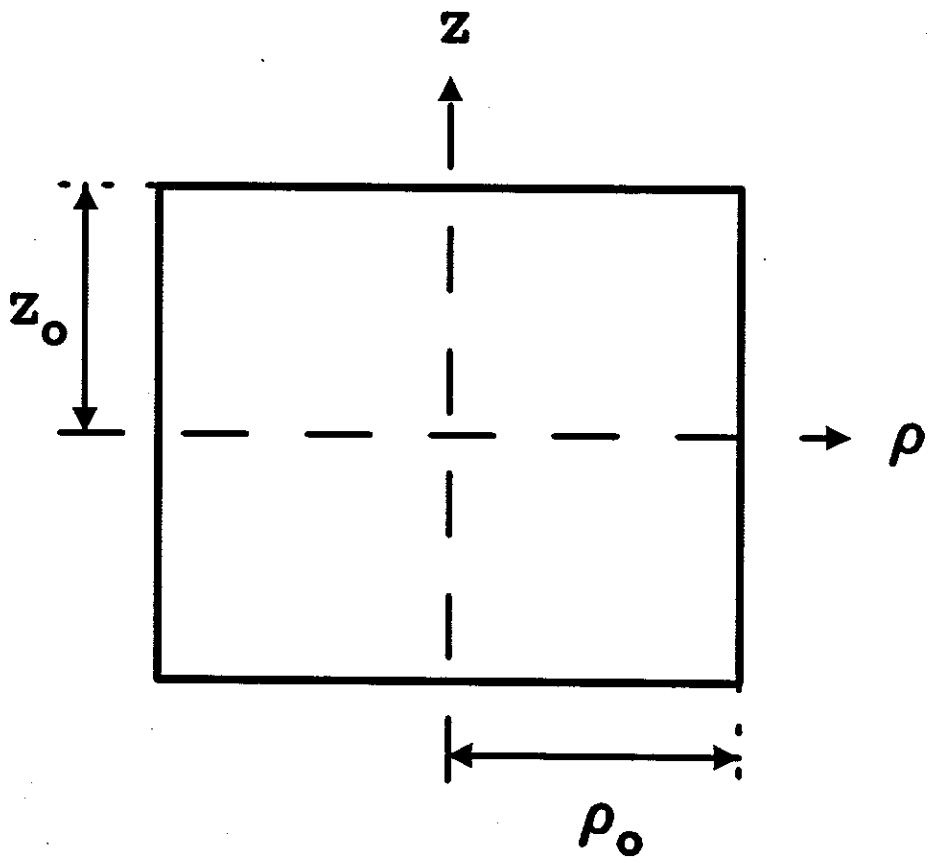

Fig. 7. Geometry of a cylindrical microwave cavity used to calculate the damping rate and frequency shift of a one-electron cyclotron oscillator which is located at the center of the cavity and oscillates about the symmetry axis of the cavity. A trap with relative geometry given by $\rho_o/z_o = 1.186$ and $z_o = 0.385$ cm is presently being used for experiments.

have to solve the system of coupled differential equations describing the interaction of the cyclotron motion with the standing waves excited in the cavity by the accelerating charged particle at the cavity center. Comparing the solution with the simple model, we choose

$$C = \frac{\rho_o^2}{8z_o} \tag{23}$$

and

$$d = \frac{2z_o}{\kappa_{n,l}}, \tag{24}$$

to maintain a close analogy when the oscillator in the model is driven. The dimensionless constant $\kappa_{n,l}$ (discussed in the next paragraph) depends upon the particular mode N,

which we identify here with the two quantum numbers $n = 0, 1, 2, ...$ and $l = 1, 2, 3, ...$ When the magnetic field is along the symmetry axis of the cavity, these two indices identify the subset of cavity modes which couple to a cyclotron oscillator located at the center of the cavity. The coupling constant is thus given by

$$\lambda_{n,l}^2 = \frac{r_e c^2}{z_o \rho_o^2} (\kappa_{n,l})^2 \tag{25}$$

from which $\gamma_N = \gamma_{n,l}$ can be calculated.

Two types of modes couple to the cyclotron motion and for both it is convenient to use $k_n = (n + 1/2)\pi/z_o$. For TE (transverse electric) modes

$$\kappa_{n,l}^2 = \frac{2}{\alpha_l^2 - 1} \frac{\alpha_l^2}{J_1(\alpha_l)^2} \tag{26}$$

$$\omega_{n,l}^2 = \left(k_n^2 + \frac{\alpha_l^2}{\rho_o^2} \right) c^2 \tag{27}$$

where α_l, defined by

$$J_1'(\alpha_l) = 0, \tag{28}$$

is the l^{th} zero of the derivative of the first order Bessel function. For TM (transverse magnetic) modes which couple to electron cyclotron motion

$$\kappa_{n,l}^2 = \frac{2 k_n^2 c^2}{\omega_{n,l}^2} \frac{1}{J_0(\beta_l)} \tag{29}$$

$$\omega_{n,l}^2 = \left(k_n^2 + \frac{\beta_l^2}{\rho_o^2} \right) c^2 \tag{30}$$

where β_l, given by

$$J_1(\beta_l) = 0, \tag{31}$$

is the l^{th} zero of the first order Bessel function. The quantum numbers n and l which we use to label the cavity modes which couple to the electron are simply related to common conventions for labeling all the modes of a cylindrical cavity. For example, in the textbook by Jackson the origin of the coordinate system is translated to the center of the bottom endcap,[22] and the TE and TM modes identified above are labeled as $TE_{1,l,2n+1}$ and the $TM_{1,l,2n+1}$, respectively. Table I gives specific values calculated for the cylindrical trap in Fig. 3.

b. Spherical Cavity

Fig. 8 represents a spherical cavity of radius ρ_o. The mode structure is particularly simple owing to the high degree of symmetry for a sphere. Only one quantum number suffices to label the modes, since only the partial waves which rotate as vectors couple to a cyclotron oscillator at the center of the cavity. Eqs.(19)-(24) still apply for the spherical cavity with $z_o = \rho_o$. The coupling parameter is given by

$$(\kappa_N)^2 = \frac{(1-\chi_N^2)^2 + \chi_N^2}{\chi_N^2 - 2}, \tag{32}$$

and the mode eigenfrequencies by

$$\omega_N = \chi_N \frac{c}{\rho_o}, \tag{33}$$

where χ_N is the Nth root of the equation

$$0 = \left(1-\chi_N^2\right)\tan(\chi_N) - \chi_N. \tag{34}$$

The eigenfrequencies and couplings of the first 25 modes are given in Table II.

c. Hyperbolic Cavity

The g-2 experiments so far have been performed in Penning traps formed from hyperbolic surfaces of revolution. Unfortunately, the microwave properties of a hyperbolic cavity are not known like those of the cylindrical or spherical cavities. The eigenfrequencies ω_N and the coupling parameter λ_N can only be obtained numerically.[13] A computer code called URMELT-T developed for accelerator studies was used.[23] The numerically calculated values for the mode frequencies and couplings in Table III are for a hyperbolic cavity closed as shown in Fig. 9. So-called endcap electrodes and ring electrodes lie approximately along hyperbola of revolution generated, respectively, by

$$z^2 = z_o^2 + \rho^2/2 \tag{35}$$

and

$$\rho^2 = \rho_o^2 + 2z^2. \tag{36}$$

An aspect ratio $\rho_o/z_o = \sqrt{2}$ was chosen, corresponding to the trap used for the measurement of the electron magnetic moment. Flat compensation ring electrodes terminate the truncation region, perpendicular to the asymptote with the perpendicular distance from the origin given by $h/z_o = 2.80$.

The numerical method was tested in computations of the eigenfrequencies and coupling parameters for the cylindrical cavity with aspect ratio $\rho_0/z_0 = 1.186$. Comparisons with the exact, analytic expressions showed that the errors in the eigenfrequencies are approximately 0.2 % on the average and do not exceed 0.4 %. The errors in the numerical

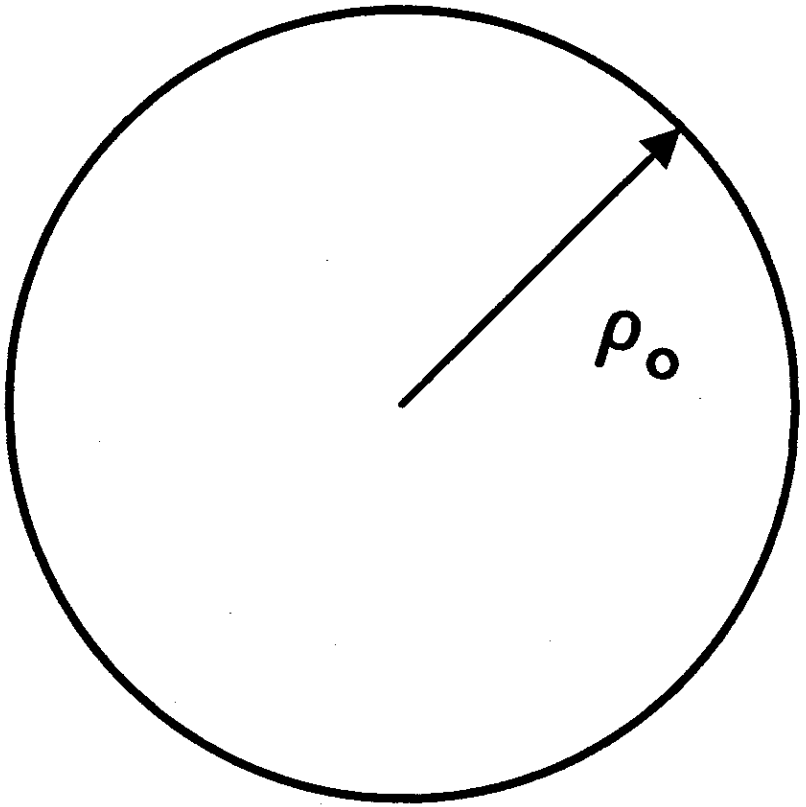

Fig. 8. Spherical cavity.

evaluation of the coupling constants are about two orders of magnitude larger. The coupling parameter for the highest frequency mode calculated (see Table III) has an 87% error because the parameters of the numerical method were not optimized. A more accurate calculation is not warranted since the actual dimensions must be known to better than 1% for the model to be directly useful. Hence, the measured values of these parameters are needed.

5. Implication for current experiments

Unfortunately, the frequencies and quality factors of the electromagnetic modes of the Penning trap used for the most accurate, electron g-2 measurements have not been measured.[2] Also, the highest precision experiment was only done for a single oscillation frequency of the electron oscillator (i.e. at only a single value of the magnetic field).

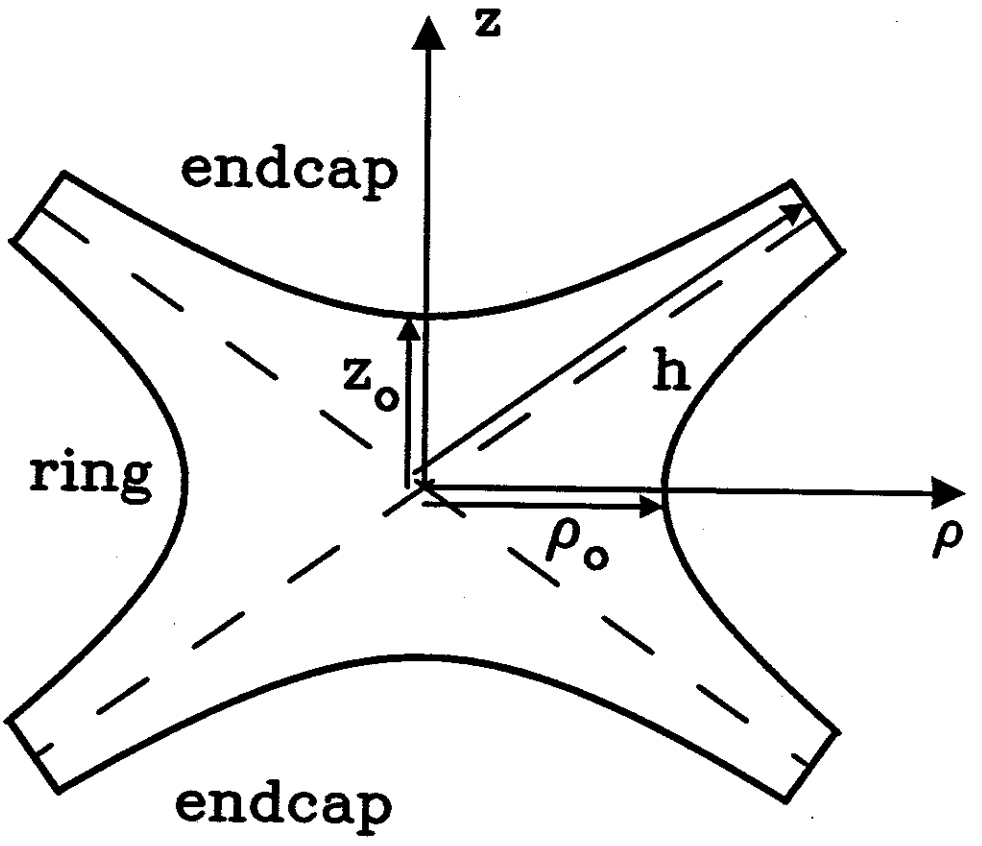

Fig. 9 Hyperbolic cavity. (From Ref. 13.)

This means that the detuning between the oscillator and the nearest cavity mode is not known at all. For an unfortunate choice of detuning, near $\delta = \pm 1$, the frequency shift could be as large as $\gamma_N/4$. From Table III we see that $\gamma_N/\gamma_c Q_N$ can be as large as 0.027 in the frequency range of interest, corresponding to a fractional frequency shift $\Delta\omega/\omega_N \approx (Q_N/20) \times 10^{-12}$. For the "reasonable" value of $Q_N = 1000$ suggested by measurements[2], this gives a possible frequency shift of 50×10^{-9}, or ten times the claimed uncertainty. For larger Q_N the maximum shift is proportionately higher.

As it happens, the experimenters were not so unlucky. A small damping rate $\gamma \approx \gamma_c/10$ was measured. Inverting Eq. (13) shows that such a shift could be caused by a detuning

$$\delta = \sqrt{\frac{\gamma_N}{\gamma} - 1} = \sqrt{\frac{\gamma_N}{\gamma_c Q_N}\frac{\gamma_c}{\gamma} Q_N - 1}. \tag{37}$$

For the illustrative mode used above, a detuning $\delta \approx \sqrt{Q_N}/2$ is required to attain the measured damping. The corresponding fractional frequency shift is $\Delta\omega/\omega \approx 0.2\sqrt{Q_N} \times$

10^{-12}. If we again use the suggested $Q_N = 1000$, this gives $\delta \approx 16$ and $\Delta\omega/\omega \approx 6 \times 10^{-12}$. From the calculated mode density for a hyperbolic cavity (see Table III) this detuning is reasonable. This fractional frequency shift is only slightly larger than the 4×10^{-12} quoted,[2] but would be higher for Q_N greater than 1000.

As illustrated in Fig. 6, including the effect of neighboring cavity modes tends to make the damping rate slightly higher than when only one mode is considered. This means that the frequency shift could tend to be slightly smaller than estimated if the cavity modes happen to be uniformly distributed in frequency. However, given the lack of knowledge of the frequencies and quality factors for the cavity modes of the real trap, we stress that these estimates are rather unreliable. We have also pointed out earlier that the coupling constants were obtained numerically with rather low accuracy. Hopefully, subsequent measurements will be done as a function of the electron's cyclotron frequency (by changing the magnetic field), within a trap cavity whose microwave properties are well measured, so that such estimates of probable measurement error are no longer required.

6. Renormalized calculation of cavity shifts

a. Renormalization

In Sec. 4, the coupling constants reported were obtained by solving the two-dimensional equation of motion for the velocity $\mathbf{v}$ of a one-electron cyclotron oscillator within a microwave cavity,

$$m\dot{\mathbf{v}} - (e/c)\mathbf{B} \times \mathbf{v} = e\mathbf{E}^{\mathbf{T}}. \tag{38}$$

The transverse radiation field within the cavity $\mathbf{E}^{\mathbf{T}}$ was taken to be the standing wave field of a particular cavity mode, generated as the accelerating particle radiates into the cavity. In this equation of motion the standing wave field acts back upon the cyclotron oscillator.

As illustrated earlier, a simple mode sum is actually not valid except for oscillator frequencies in close proximity to the resonant frequency of a high Q cavity mode. To understand this, we note that the standing wave field is actually composed of two contributions

$$\mathbf{E}^{\mathbf{T}} = \mathbf{E}_{self} + \mathbf{E}', \tag{39}$$

the self-field $\mathbf{E}_{self}$ radiated directly by the oscillator (as if into free space) and the reflected field $\mathbf{E}'$ which is reflected from the cavity walls. The back reaction of a self-field upon the accelerating charge which is radiating, is well known to lead to difficulties and divergences in classical electricity and magnetism.[24] In our particular situation, the real part of the mode sum [Eq. (19)] diverges when the sum includes all the cavity modes.

Given the usefulness of the simple model and mode sum in certain circumstances, it is instructive to see how the divergences arise and can be partially circumvented in this model. Consider first the case that the cyclotron oscillator's frequency is near enough to the eigenfrequencies of several cavity modes to be dominated by these modes. In the standing waves of these modes, the self-field is much smaller than the built up reflected wave in the cavity and can be neglected. The simple model thus describes quite well the contributions of these dominant modes. Cavity modes far from resonance with the cyclotron oscillator

contribute relatively little to the damping or to the frequency shift of the oscillator and thus can be neglected. Neglecting the off-resonant contributions is essential here, since an unrenormalized calculation of these contributions overstates them and leads to a divergent result when the mode sum includes all cavity modes.

The situation is quite different when the cyclotron oscillator is not close in frequency to the resonant frequency of any cavity mode. A number of off-resonant cavity modes make small contributions to the damping of the oscillator as well as to shifting its frequency. Typically, including the contributions of more nearest neighbor modes in the mode sum initially improves the accuracy of the calculated frequency shift. The difficulty is that for off resonant modes, the Fourier component of the standing wave fields at the electron frequency contains a non-negligible amount of self-field. As mentioned above, these self-fields are the problem. For any particular off-resonant mode, the contribution to the frequency shift of the electron oscillator is slightly overstated due to self-field in the standing wave. The overstated contributions add up as the contributions from many modes are included. Optimal use of the simple, mode sum model thus requires a careful choice of the number of cavity modes included in the sum. Beyond a certain number of terms, the real part of the mode sum will start to diverge. Eventually, the mode sum over an infinite number of such small contributions diverges. It is difficult to establish the optimum number of terms or the accuracy of the truncated mode sum except by comparison to a calculation which avoids the divergences entirely and which is the subject of the remainder of this section.

For a correctly renormalized calculation, the self-field term is replaced by a radiation damping term for radiation into free space (with damping time γ_c discussed earlier) and only the transverse reflected field $\mathbf{E}'$ acts back upon the cyclotron oscillator,

$$\dot{\mathbf{v}} - \omega_c \times \mathbf{v} + \frac{1}{2}\gamma_c \mathbf{v} = (e/m)\mathbf{E}'. \tag{40}$$

Only in special cases is it possible to separate the reflected field and the self-field which together make up the standing wave. The high degree of symmetry for a spherical cavity (Sec. 6.1) makes the removal of the self-field relatively simple because the free-space radiation from the oscillator at the center contains only outgoing spherical waves, easily distinguished from the reflected waves. A cylindrical cavity (Sec. 6.2) has less symmetry, but the separation can still be accomplished by using image charges to satisfy the cavity boundary conditions. The reflected field is thus clearly distinguished as the field of the images. Unfortunately, for a hyperbolic cavity (which corresponds to the trap within which the electron's magnetic moment was measured) a separation of self and reflected fields is completely intractable. Finite mode sums as done in the simple model are the only possibility. Comparisons of a mode sum and a complete calculation for the cylindrical cavity are used to estimate the optimal number of terms to be included in the finite mode sum. To set up a framework for specific calculations, we use the radiation gauge. The transverse electric fields $\mathbf{E}^{\mathbf{T}}$, $\mathbf{E}_{\mathbf{self}}$ and $\mathbf{E}'$ are thus time derivatives of vector potentials. These vector potentials, in turn, can be written in terms of Green's functions. For example, the standing wave field $\mathbf{E}^{\mathbf{T}}$ can be written as

$$\mathbf{E}^{\mathrm{T}}_{\mathbf{k}}(t,\mathbf{r}) = -\frac{\partial}{\partial t}\int dt' \sum_{l=1}^{3} D_{kl}(t-t';\mathbf{r},\mathbf{r}(t'))ev_l(t')/c^2. \tag{41}$$

It is convenient to Fourier transform $D_{kl}(t-t';\mathbf{r},\mathbf{r}')$, according to

$$D_{kl}(t-t';\mathbf{r},\mathbf{r}') = \int \frac{d\omega}{2\pi} e^{-i\omega(t-t')} \tilde{D}_{kl}(\omega;\mathbf{r},\mathbf{r}'). \tag{42}$$

From the wave equation for the vector potential in the radiation gauge, with a point current source, we obtain

$$\left(-\nabla^2 - k^2\right) \tilde{D}_{kl}(\omega;\mathbf{r},\mathbf{r}') = 4\pi \left[1 - \nabla \frac{1}{\nabla^2} \nabla\right]_{kl} \delta(\mathbf{r}-\mathbf{r}'). \tag{43}$$

The gradient operator ∇ and the inverse $1/\nabla^2$ in the square brackets insure that only transverse radiation fields are being considered. Of course, the Green's function must satisfy the cavity boundary conditions as well.

The self-field $\mathbf{E_{self}}(t,\mathbf{r})$ can be similarly written in terms of the free space Green's function $D^{self}_{kl}(t-t';\mathbf{r},\mathbf{r}')$ or its Fourier transform $\tilde{D}^{self}_{kl}(\omega;\mathbf{r},\mathbf{r}')$. The latter is a solution to the same wave equation (43), but with boundary conditions appropriate to free space. What we are most interested in, however, is the reflected field $E'(t,\mathbf{r})$ which is needed to solve the renormalized equation of motion (40) for the cyclotron oscillator in a cavity. As above, we can write the reflected wave in terms of $D'_{kl}(t-t';\mathbf{r},\mathbf{r}')$ and its Fourier transform $\tilde{D}'_{kl}(\omega;\mathbf{r},\mathbf{r}')$. This Fourier transform is a solution of the homogeneous equation

$$\left(-\nabla^2 - k^2\right) \tilde{D}'_{kl}(\omega;\mathbf{r},\mathbf{r}') = 0, \tag{44}$$

since the sources of the reflected waves are not located within the cavity. $\tilde{D}'_{kl}(\omega;\mathbf{r},\mathbf{r}')$ is thus the unique modification which must be added to the free space Green's function to obtain the Green's function for the standing waves which satisfies the cavity boundary conditions.

The desired damping rates and frequency shifts for the cyclotron oscillator can be simply expressed in terms of the modification to the Green's function. We use the Fourier expansion of $D'_{kl}(t-t';\mathbf{r},\mathbf{r}')$ in the renormalized equation of motion and use the complex notation for the velocities $v(t) = v_x(t) - iv_y(t) \sim e^{-i\omega t}$, which includes the assumption that the oscillator has a well defined frequency. If we restrict our attention to a cyclotron oscillator located at the center of the cavity ($\mathbf{r} = 0 = \mathbf{r}'$) we obtain

$$\omega - \omega_c + i\gamma_c/2 = -\omega r_0 \tilde{D}'_{xx}(\omega;0,0). \tag{45}$$

The simplicity of the right-hand side of Eq.(45) results from the axial symmetry which implies that $\tilde{D}'(\omega;0,0)$ is proportional to the unit dyadic in the xy plane, with the proportionality constant $\tilde{D}'_{xx}(\omega;0,0) = \tilde{D}'_{yy}(\omega;0,0)$. In general, the Green's function modification $\tilde{D}'_{xx}(\omega;0,0)$ is a complex number, and thus the presence of the cavity modifies the cyclotron decay constant away from its free-space value γ_c. In the limit of a perfect cavity with perfectly conducting walls, the imaginary part of $\tilde{D}'_{xx}(\omega;0,0)$ cancels γ_c exactly. In this limit there is no decay of the cyclotron motion because there is no dissipative process to absorb the energy.

b. Spherical cavity

A notable feature of the spherical cavity is that the effects of dissipation can be treated exactly. Because of the spherical geometry, application of the boundary conditions appropriate for cavity walls with finite conductivity,[15] does not mix the modes and leads to

$$\omega - \omega_c' + \frac{1}{2}i\gamma_c = \frac{1}{2}i\gamma_c \left[\frac{(1 - i\eta k\rho_o)h_1(k\rho_o) + (k\rho_o)h_1'(k\rho_o)}{(1 - i\eta k\rho_o)j_1(k\rho_o) + (k\rho_o)j_1'(k\rho_o)} - \frac{3}{2}i\frac{1}{(k\rho_o)^3} \right], \tag{46}$$

where $k = \omega/c$ is the wave number at frequency ω. Here, η relates the electric and magnetic field components just outside the surface of the lossy conductor

$$\mathbf{E}_\parallel = \eta \mathbf{n} \times \mathbf{B}_\parallel, \tag{47}$$

where $\mathbf{n}$ is the outward unit normal to the surface. In terms of the magnetic permeability of the conductor μ and the skin depth δ_s,

$$\eta = \mu(1 - i)k\delta_s/2. \tag{48}$$

In Eq. (46) we use the usual notation $j_1(x)$ for the spherical Bessel function and $h_1(x)$ for the outgoing wave spherical Hankel function, both of order one. The prime denotes a derivative with respect to the argument.

Since the dissipative effects given in Eq.(46) only approximately model an actual trap, and since dissipative effects are generally very small except near a cavity resonance, it suffices to adopt the simple procedure of replacing ω by the complex extension $\omega \to \omega(1 + i/2Q)$, where Q is an average quality factor for the frequency range of interest. In this way, we obtain from Eq.(46)

$$\omega - \omega_c' = \Delta\omega - \frac{i}{2}\gamma = -\frac{1}{2}i\gamma_c + \frac{1}{2}i\gamma_c \left[\frac{(1 - z^2)\cos z + z\sin z}{(1 - z^2)\sin z - z\cos z} + \frac{3}{2z^3} \right] \tag{49}$$

where

$$z = \frac{\omega\rho_o}{c}\left[1 + \frac{i}{2Q}\right] \tag{50}$$

and explicit forms for the Bessel functions have been used.

In Fig. 10, we highlight the important features of this result and compare directly with those of the cylindrical cavity (to be discussed). The cavity shifts are plotted against the dimensionless variable $\xi = 2\rho_o/\lambda$ for the spherical cavity, while for the cylindrical cavity we use $\xi = 2z_o/\lambda$ where $2z_o$ is the length of the cylinder. We take ρ_o to be also the radius of the cylinder, and set $z_o = 2\rho_o/3$ so that both cavities have the same volume. We use a rather low value, $Q = 100$, so as to more clearly exhibit the structure. The regularity of the spherical modes (thick line) is set against the complicated mode structure of the cylindrical cavity (thin line). The cylindrical-cavity mode spacing steadily decreases as the frequency increases, with considerable merging of the modes giving rise to a complicated fine structure. In contrast, the modes of the spherical cavity are quite evenly spaced with a larger spacing, and although there is a broadening of the widths

with increasing frequency, with an accompanying decrease in the height of the peaks, the dispersive and absorptive structure maintain a distinct corelation with one another and to the normal resonant frequencies. But because the spherical-cavity mode spacing is larger than that of the cylinder, while the average total "oscillator strength" of the two cavities must be the same, the effects are much larger for the sphere. Roughly speaking, the cavity reflection field from a spherical surface is optimally focused to the center of the trap and thus produces a stronger effect.

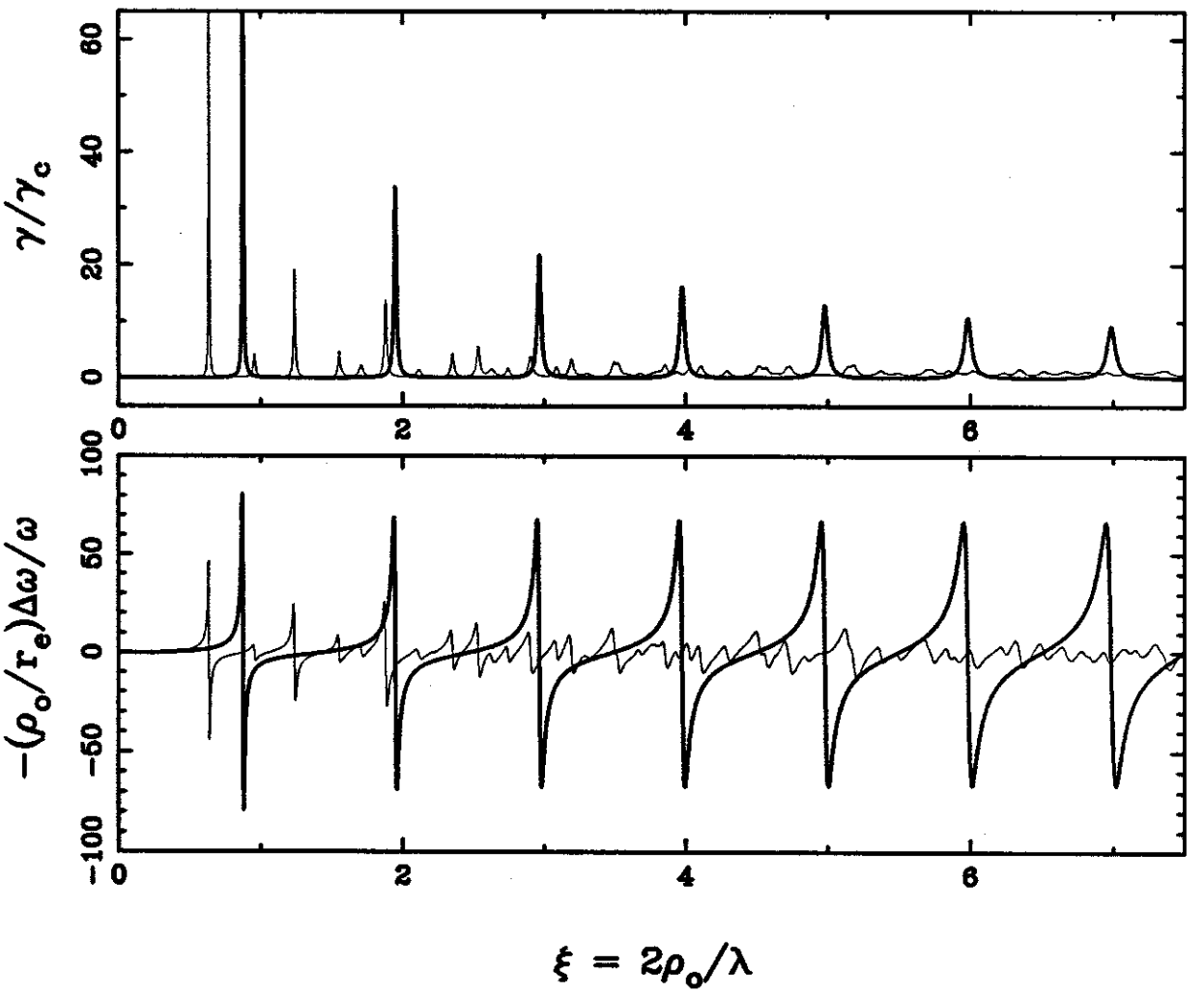

Fig. 10. Damping time and frequency shift as a function of normalized frequency ξ, for a spherical cavity (thick line) and for a cylindrical cavity of the same volume (thin line), both with $Q = 100$. (From Ref.15.)

6.3 Cylindrical cavity

To get the renormalized alteration for the cylindrical cavity, we note that the limit in which the cavity radius goes to infinity yields a geometry with two parallel, infinite

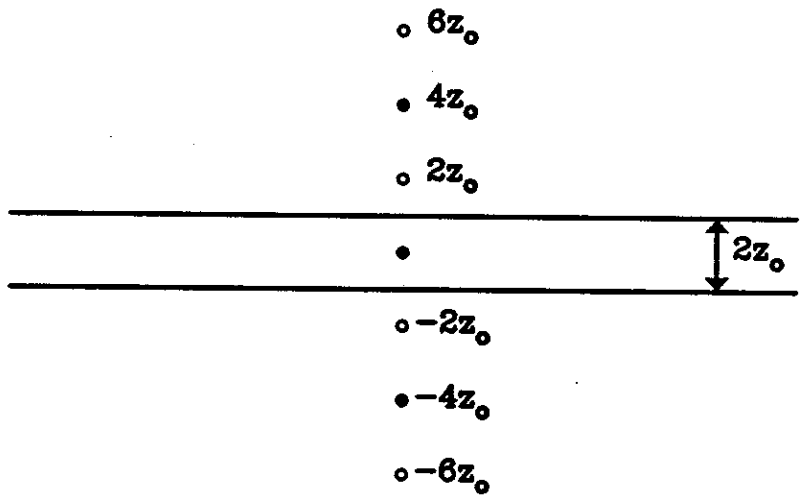

Fig. 11. Image charges for an electron midway between two parallel plates.

conducting planes a distance $2z_o$ apart. Thus we express the Green's function as the sum of the Green's function for the parallel plate problem plus the solution to the homogeneous wave equation which corrects for the presence of the cylindrical side wall. This gives

$$\omega - \omega_c' = \Delta\omega - \frac{i}{2}\gamma = -\frac{i}{2}\gamma_c + \omega\left[\Sigma_P(\omega + \frac{i}{2}\Gamma) + \Sigma_S(\omega + \frac{i}{2}\Gamma)\right] \tag{51}$$

where Σ_P is the parallel-plate contribution to the renormalized green's function alteration, and Σ_S is the correction due to the cylindrical side of the cavity. Since the Green's function for the two-parallel plate geometry can be expressed as an infinite sum of image contributions as shown in Fig. 11, the removal of the self-field term is now trivial: the direct contribution is omitted from the sum. Using the method of images we obtain

$$\Sigma_P(\omega) = \frac{r_e}{z_o}\ln\left[1 + e^{2i\omega z_o/c}\right] - \frac{r_e}{z_o}\sum_{n=1}^{\infty}(-1)^n\left[e^{2in\omega z_o/c}\left(\frac{ic}{2n^2 z_o\omega} - \frac{c^2}{4n^3 z_o^2\omega^2}\right) + \frac{c^2}{4n^3 z_o^2\omega^2}\right]. \tag{52}$$

The alteration of the Green's function brought about by the presence of the circular side can be expressed in terms of an infinite sum over the axial standing waves that fit between the two endcap planes. The wave numbers of the waves that do not vanish at the midplane location of the charged particle are given by

$$k_n = (n + \frac{1}{2})\pi/z_o, \tag{53}$$

where $n = 0, 1, 2, \ldots$. With ω below the first axial threshold, $\xi < \frac{1}{2}$, the radial waves are exponentially damped with the damping constant

$$\mu_n = (k_n^2 - \omega^2/c^2)^{1/2}. \tag{54}$$

In terms of this decomposition, the cavity side addition to the complex frequency shift (47) is given by

$$\Sigma_S(\omega) = -\frac{r_e}{z_o}\sum_{n=0}^{\infty}\left\{\frac{K_1'(\mu_n\rho_o)}{I_1'(\mu_n\rho_o)} + \frac{k_n^2c^2}{\omega^2}\left[\frac{K_1(\mu_n\rho_o)}{I_1(\mu_n\rho_o)} - \frac{K_1(k_n\rho_o)}{I_1(k_n\rho_o)}\right]\right\}, \tag{55}$$

where the prime denotes a derivative. The first ratio of Bessel functions is the TE contribution, the terms in the large parentheses are the TM contribution. When ω is near the nth threshold, μ_n becomes small, and the nth term in the sum (55) has a large logarithmic contribution that cancels the large logarithm in the parallel plate term. As ω passes the threshold, μ_n becomes a negative imaginary number. In the limit of vanishing dissipation ($\Gamma = 0$), the imaginary part of the Bessel function ratios cancels the imaginary part of the parallel plate term. Past a threshold, the Bessel functions in the denominator can vanish, producing poles corresponding to the normal modes of the cavity. The replacement $\omega \to \omega + i\Gamma/2$ changes these poles into Lorentzian forms of width Γ. The sum in (55) converges very rapidly; for large n, $\mu_n \sim k_n \sim n\pi/z_o$, and it is exponentially damped. Thus the sum is easily calculated on a digital computer. Adding the result to the previous parallel plate contribution gives the complete shift of Eq.(51).

We use the aspect ratio $\rho_o/z_o = 1.186$ for the cylindrical cavity, which has been employed to demonstrate the possibility of the cylindrical geometry for a Penning trap. Experiments are generally performed in the region $3.5 < \xi < 4.5$, and Fig. 12 illustrates the result in this region. But before passing to this, we note that the various cavity modes have different quality factors. In the region that we are considering, the quality factors for perfect cylindrical geometry for the TE modes Q_E are , to within about 10 percent, twice the quality factors Q_M of the TM modes. We approximately account for this difference in cavity widths by using the complex frequency $\omega(1+i/2Q_E)$ in the TE denominator function $I_1'(\mu_n\rho_o)$ in Eq.(55), while all the other complex frequencies are given by $\omega(1 + i/2Q_M)$, with $Q_M = Q_E/2$. (By keeping all the other complex frequencies the same, we preserve the threshold cancellation discussed above, as we must.) Actual cylindrical penning traps contain holes and slits, and the quality factors are difficult to calculate accurately. Thus, although one could alter the individual modes in the interval $3.5 < \xi < 4.5$ by putting in the exact widths, this is not warranted by the uncertainty in our knowledge of the widths of the experimental traps. Thus we use the simple substitution described above to compute the decay constants and frequency shifts plotted in Fig. 12 for a typical quality factor $Q_E = 1000$. A $Q \gtrsim 1000$ is required to make possible the decrease in the damping constant by the factor of 10 which has been observed.[2]

7. Summary and future prospects

Cavity shifts of the cyclotron frequency of a one-electron cyclotron oscillator presently limit the accuracy of measurements of the anomalous magnetic moment of the electron. A substantial change in the electron's damping rate has been observed,[5] but a frequency shift has not been observed directly. In fact, little is known experimentally about the microwave

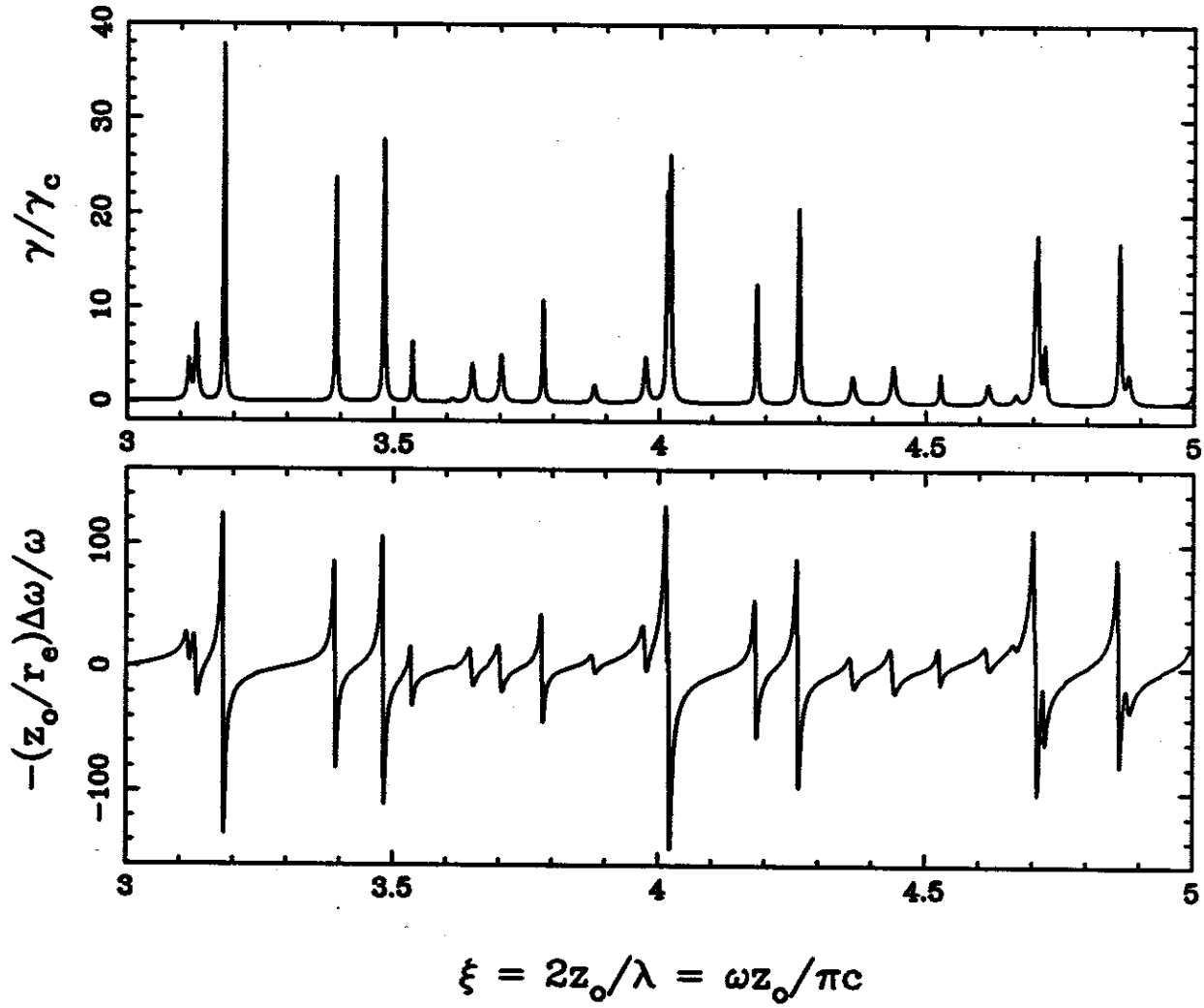

Fig. 12. Damping time and frequency shift as a function of normalized frequency ξ of the cyclotron oscillator, for the cylindrical cavity in Fig. 7 with $Q = 1000$.

properties of the cavities in which magnetic moment measurements have been done. On the theoretical side, a simple model whereby the electron is coupled to a single cavity mode illustrates the characteristic damping and frequency shift of the electron oscillator. Moreover, the simple model can be quantitatively useful when the electron oscillator and a cavity mode are nearly resonant. When the electron oscillator is not resonant with a cavity mode, however, a properly renormalized calculation is required for a precise description. Such a calculation can be done for cylindrical and spherical cavities, but not for hyperbolic cavities (which correspond most closely to traps used for precise measurements so far).

Two experimental directions are being pursued. One is to deliberately make the trap of lossy materials[2] to minimize the radiation which reflects from the cavity walls and acts back upon the oscillator. A possible alternative might be to make trap electrodes which lie along a cylinder, but with completely open ends[25] through which radiation can escape. The second direction is to use the cavity to control the radiation, by tuning the electron oscillator's frequency as close as desired to the eigenfrequency of a high Q cavity mode. A

cylindrical trap cavity[14] is promising here (compared to the hyperbolic traps) because a proper renormalized calculation can be done for this geometry and because it is easier to build a high Q cavity of this geometry. Moreover, it has recently been demonstrated that a single electron can be confined and interrogated within such a cavity just as well as in the traditional hyperbolic geometry. Hopefully the perturbations due to slits in the cavity (needed to make a particle trap) are very small, with radiation losses kept small by choke flanges, but this remains to be seen. Prospects seem good for a systematic experimental study of the damping and frequency shifts of a one-electron cyclotron oscillator within a well-characterized microwave cavity.

8. References

1. The theory is described in the article by T. Kinoshita in this volume.
2. The experiment is described in the article by R.S. Van Dyck, Jr. in this volume.
3. L.S. Brown, "Line Shape for a Precise Measurement of the Electron's Magnetic Moment", Phys. Rev. Lett. **52**, 2013 (1984). "Geonium Lineshape", Ann. Phys. **159**, 62 (1985).
4. G. Gabrielse, H. Dehmelt and W. Kells, "Observation of a Relativistic, Bistable Hysteresis in the Cyclotron Motion of a Single Electron", Phys. Rev. Lett. **54**. 537 (1985).
5. G. Gabrielse and H.G. Dehmelt, "Observation of Inhibited Spontaneous Emission", Phys. Rev. Lett. **55**, 67 (1985).
6. H.G. Dehmelt, "g-Factor of Electron Centered in a Symmetric Cavity", Proc. Nat. Acad Sci. U.S.A. **81**, 8037 (1984). See also the erratum in Proc. Nat. Acad. Sci. U.S.A. **82**, 6366 (1985).
7. L.S. Brown, G. Gabrielse, K. Helmerson and J. Tan, "Cyclotron Motion in a Microwave Cavity: Possible Shifts of the Measured Electron g Factor", Phys. Rev. Lett. **55**, 44 (1985).
8. E.M. Purcell, "Spontaneous Emission Probabilities at Radio Frequencies", Phys. Rev. **69**, 681 (1946).
9. D. Kleppner, "Inhibited Spontaneous Emission", Phys. Rev. Lett. **47**, 233 (1981).
10. D. Kleppner, in *Atomic Physics and Astrophysics*, edited by M. Chretien and E. Lipworth (Gordon & Breach, NY, 1971).
11. Reviewed by S. Haroche and D. Kleppner,"Cavity Quantum Electrodynamics", Physics Today, Jan. 1989, p. 24. See also E.A. Hinds, "Cavity Quantum Electrodynamics", in Adv. At. Mol. Opt. Phys. **87** (1990).
12. L.S. Brown and G. Gabrielse, "Geonium Theory: Physics of an Electron or Ion in a Penning Trap", Rev. Mod. Phys. **58**, 233 (1986).
13. L.S. Brown, G. Gabrielse, J. Tan and K.C.D. Chan, "Cyclotron Motion in a Penning-trap Microwave Cavity", Phys. Rev. A **37**, 4163 (1988).
14. L.S. Brown, G. Gabrielse, K. Helmerson, J. Tan, "Cyclotron Motion in a Microwave Cavity: Lifetime and Frequency Shifts", Phys. Rev. A **32**, 3204 (1985).
15. L.S. Brown, K. Helmerson and J. Tan, "Cyclotron Motion in a Spherical Microwave Cavity", Phys. Rev. A. **34**, 2638 (1986).

16. D.G. Boulware, L.S. Brown and T. Lee, "Apparatus-dependent contributions to $g-2$?", Phys. Rev. D **32**, 729 (1985).
17. G. Gabrielse and F.C. MacKintosh, "Cylindrical Penning Traps with Orthogonalized Anharmonicity Compensation", Int. J. of Mass Spec. and Ion Proc. **57**, 1 (1984).
18. J. Tan and G. Gabrielse,"One Electron in an Orthogonalized Cylindrical Penning Trap," Appl. Phys. Lett. **55**, 2144 (1989).
19. R.S. Van Dyck, Jr., F.L. Moore, D.L. Farnham, P.B. Schwinberg and H.G. Dehmelt, "Microwave-cavity Modes Directly Observed in a Penning Trap", Phys. Rev. A **36**, 3455 (1987).
20. It is customary in microwave electronics to present information in the form of equivalent circuits. See for example Robert Beringer, "Resonant Cavities as Microwave Circuit Elements", in *Principles of Microwave Circuits* pp. 207 - 239, edited by C.G. Montgomery, R.H. Dicke, E.M. Purcell (MIT Rad. Lab. Series) (McGraw, NY, 1948).
21. This is the definition of $(\lambda_N)^2$ used in Ref. 14 [Phys. Rev. A **32**, 3204 (1985)]. It is smaller than the dimensionless $(\lambda_N)^2$ used in Ref. 13 [Phys. Rev. A **37**, 4163 (1988)] by a factor $\omega_N^2 r_e/z_o$.
22. J.D. Jackson, *Classical Electrodynamics*, 2nd Edition (Wiley, New York).
23. The computer code is the Los Alamos National Laboratory-Deutsches Elecktronen-Synchotron (LANL-DESY) program URMELT-T. The LANL-DESY program called URMEL is described by T. Weiland, DESY report No. 82-24, 1982 (unpublished).
24. See e.g., Panovsky and M. Phillips, *Classical Electricity and Magnetism*, 2nd edition, (Addison-Wesley, Reading, MA., 1962) chapters 21 and 22 , or Ref. 19, Chapter 17.
25. G. Gabrielse, L. Haarsma and S.L. Rolston, "Open-endcap Penning Traps for Precision Experiments", Intl. J. of Mass Spec. and Ion Proc. **88**, 319 (1989).

Table I. Mode structure for a cylindrical cavity with $\rho_0/z_0 = 1.186$

$N = (n,l)$	$\xi_N = z_o\omega_N/\pi c$	$(z_o/r_e)(\lambda_N/\omega_N)^2$	$\gamma_N/(Q_N\gamma_c)$	TYPE
0, 1	0.702985	1.2213	0.8295	TE
0, 1	1.143497	0.1299	0.0542	TM
0, 2	1.515745	0.5425	0.1709	TE
1, 1	1.579300	0.2420	0.0732	TE
1, 1	1.818677	0.1827	0.0480	TM
0, 2	1.948165	0.0278	0.0068	TM
1, 2	2.073037	0.2900	0.0668	TE
0, 3	2.344983	0.3556	0.0724	TE
1, 2	2.407353	0.1072	0.0213	TM
2, 1	2.548370	0.0929	0.0174	TE
2, 1	2.703254	0.1039	0.0184	TM
1, 3	2.738420	0.2608	0.0455	TE
0, 3	2.775854	0.0097	0.0017	TM
2, 2	2.880535	0.1502	0.0249	TE
1, 3	3.115344	0.0552	0.0085	TM
2, 2	3.129752	0.1042	0.0159	TM
0, 4	3.181306	0.2634	0.0395	TE
2, 3	3.391009	0.1701	0.0239	TE
1, 4	3.481481	0.2200	0.0302	TE
3, 1	3.534712	0.0483	0.0065	TE
0, 4	3.610725	0.0044	0.0006	TM
3, 1	3.647956	0.0614	0.0080	TM
2, 3	3.702076	0.0769	0.0099	TM
3, 2	3.781201	0.0872	0.0110	TE
1, 4	3.877800	0.0301	0.0037	TM
3, 2	3.974336	0.0785	0.0094	TM
2, 4	4.015060	0.1654	0.0197	TE
0, 5	4.020443	0.2089	0.0248	TE
3, 3	4.183174	0.1118	0.0128	TE
1, 5	4.261919	0.1859	0.0208	TE
2, 4	4.363179	0.0521	0.0057	TM
3, 3	4.439073	0.0729	0.0078	TM
0, 5	4.448730	0.0024	0.0003	TM
4, 1	4.527051	0.0295	0.0031	TE
4, 1	4.616014	0.0396	0.0041	TM
1, 5	4.668105	0.0177	0.0018	TM
3, 4	4.703266	0.1205	0.0122	TE
2, 5	4.707861	0.1524	0.0155	TE
4, 2	4.722021	0.0559	0.0057	TE
0, 6	4.860961	0.1730	0.0170	TE

Table II. Mode structure for a spherical cavity

N	$\xi_N = \rho_o\omega_N/\pi c$	$(\rho_o/r_e)(\lambda_N/\omega_N)^2$	$\gamma_N/(Q_N\gamma_c)$
1	0.873349	1.606573	0.878323
2	1.947027	1.371989	0.336450
3	2.965571	1.349238	0.217231
4	3.974397	1.342053	0.161228
5	4.979597	1.338849	0.128374
6	5.983033	1.337140	0.106708
7	6.985475	1.336119	0.091325
8	7.987301	1.335461	0.079831
9	8.988719	1.335012	0.070913
10	9.989851	1.334691	0.063792
11	10.990776	1.334455	0.057972
12	11.991547	1.334275	0.053127
13	12.992198	1.334135	0.049030
14	13.992757	1.334024	0.045520
15	14.993240	1.333935	0.042480
16	15.993663	1.333862	0.039820
17	16.994036	1.333802	0.037475
18	17.994368	1.333751	0.035390
19	18.994665	1.333708	0.033525
20	19.994932	1.333671	0.031847
21	20.995173	1.333640	0.030329
22	21.995393	1.333613	0.028949
23	22.995593	1.333589	0.027690
24	23.995777	1.333568	0.026535
25	24.995946	1.333550	0.025473

Table III. Mode structure for a hyperbolic cavity

N	$\xi_N = z_o\omega_N/\pi c$	$(z_o/r_e)(\lambda_N/\omega_N)^2$	$\gamma_N/(Q_N\gamma_c)$
1	0.443	0.30	0.32
2	0.663	0.71	0.51
3	0.926	0.12	0.061
4	1.184	0.47	0.19
5	1.291	0.049	0.018
6	1.337	0.043	0.015
7	1.469	0.065	0.021
8	1.565	0.27	0.083
9	1.693	0.042	0.012
10	1.729	0.040	0.011
11	1.740	0.32	0.087
12	1.898	0.071	0.018
13	1.971	0.0029	0.00070
14	2.021	0.034	0.0081
15	2.079	0.34	0.079
16	2.147	0.011	0.0025
17	2.237	0.018	0.0039
18	2.299	0.12	0.025
19	2.352	0.079	0.016
20	2.405	0.082	0.016
21	2.471	0.048	0.0093
22	2.534	0.0032	0.00060
23	2.562	0.066	0.012
24	2.669	0.0052	0.00093
25	2.693	0.28	0.050
26	2.730	0.14	0.024
27	2.739	0.0058	0.0010
28	2.836	0.11	0.019
29	2.894	0.0034	0.00056
30	2.954	0.080	0.013
31	2.988	0.11	0.017
32	3.075	0.043	0.0066
33	3.105	0.015	0.0022
34	3.137	0.057	0.0087
35	3.161	0.0015	0.00022
36	3.177	0.053	0.0079
37	3.285	0.00015	0.000021
38	3.308	0.18	0.026
39	3.324	0.13	0.018
40	3.374	0.018	0.0025
41	3.446	0.072	0.010
42	3.458	0.00050	0.000069
43	3.514	0.11	0.014
44	3.571	0.20	0.027
45	3.711	0.025	0.0032